Chemical Engineering Journal 345 (2018) 389–394

Contents lists available at ScienceDirect

Chemical Engineering Journal

journal homepage: www.elsevier.com/locate/cej

Highly ordered Au-Ag alloy arrays with tunable morphologies for surface enhanced Raman spectroscopy

Zhezhe Wang[a,b,c,*,1], Xin Wen[a,1], Zhuohong Feng[a,b,c], Lin Lin[a,b,c], Ruihua Liu[a], Pingping Huang[a], Guilin Chen[a,b,c], Feng Huang[a,b,c], Zhiqiang Zheng[a,b,c,*]

[a] College of Physics and Energy, Fujian Normal University, Fuzhou 350117, China
[b] Fujian Provincial Key Laboratory of Quantum Manipulation and New Energy Materials, Fuzhou 350117, China
[c] Fujian Provincial Collaborative Innovation Center for Optoelectronic Semiconductors and Efficient Devices, Xiamen 361005, China

HIGHLIGHTS

- A flexible approach for fabricating the highly ordered Au-Ag alloy arrays for SERS is proposed.
- The morphologies of the Au-Ag alloy are regulated via adjusting the nucleation and growth processes.
- The maximum SERS is observed for the flower-like Au-Ag alloy with a small amount of Au (12%).

GRAPHICAL ABSTRACT

Highly ordered Au-Ag alloy arrays with tunable morphologies for SERS substrates are fabricated by a controllable and reproducible approach combining electrochemical reaction self-assembly and photolithography.

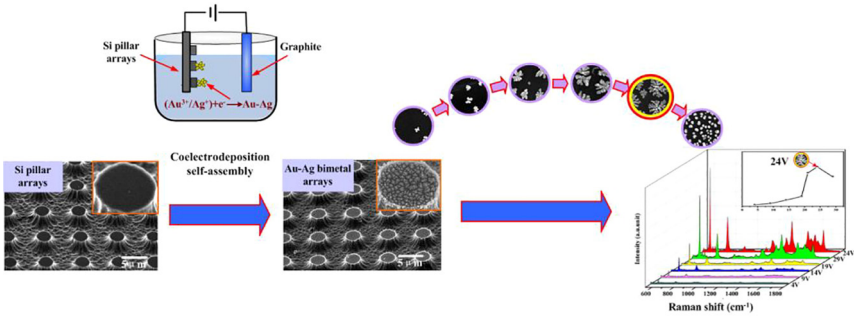

ARTICLE INFO

Keywords:
Au-Ag alloy arrays
SERS
Flower-like structures
Self-assembly
Photolithography

ABSTRACT

A simple approach combining electrochemical reaction self-assembly and photolithography has been proposed for the controlled and reproducible fabricating the highly ordered Au-Ag alloy arrays for SERS. The nucleation and growth processes of the Au-Ag alloy are adjusted easily via changing the applied voltage and reaction time to obtain the flower-like hierarchy nanostructure, which show the strongest SERS properties due to the wealthy Raman "hot spots" provided by the corners and edges in much-branched flower structure. Moreover, the maximum SERS is observed for the Au-Ag alloy with a small amount of Au (12%), which can lead to a charge separation and favor the probe molecules adsorption to the silver domains. By using these flower-like Au-Ag alloy arrays, the Rhodamine 6G (R6G) with the concentration of as low as 10^{-12}M can be detected easily in this study, which would be very promising for the applications in biosensors and nanodevices with molecule-level detection.

1. Introduction

Since Surface-Enhanced Raman scattering (SERS), where a Raman signal is strongly enhanced when molecules are attached to the rough surface of some noble metal nanostructures, was observed in 1970s [1], there has been a tremendous amount of researches focused on SERS due

* Corresponding authors at: College of Physics and Energy, Fujian Normal University, Fuzhou 350117, China.
E-mail addresses: zzwang@fjnu.edu.cn (Z. Wang), zqzheng@fjnu.edu.cn (Z. Zheng).
[1] These authors contributed to the work equally and should be regarded as co-first authors.

https://doi.org/10.1016/j.cej.2018.03.192
Received 17 January 2018; Received in revised form 30 March 2018; Accepted 31 March 2018
Available online 01 April 2018
1385-8947/ © 2018 Elsevier B.V. All rights reserved.

to its single-molecule sensitivity and excellent fingerprint effect for practical applications in detection and recognition technology [2–4]. Generally, SERS-active substrates have been restricted to some noble metals materials, especially the Silver (Ag) and Gold (Au), which have been widely used in SERS studies due to the higher plasmonic enhancement and better biocompatibility [5–9]. Compared with the single metallic Ag substrate with weak stability against oxidation, and Au with the relatively weak SERS activity, Au/Ag alloy materials system is a preferable choice and very promising for the enhancement of SERS signal and application in analytical technique, because it exhibits both the dramatic Raman enhancement and good compatibility [10].

In addition to further optimize SERS effect, recently, benefiting from the advance in micro/nano - fabrication techniques, patterned noble metal arrays substrates applied for SERS have attracted much more attention [11–12]. Compared with the flat noble metal, the metallic arrays can provide broadband, wide-angle and large electromagnetic (EM) fields excitation and surface plasmon resonances (SPRs), and hence to process much more Raman “hot spots”, which can significantly amplify Raman scattering intensity of the attached molecules [13–16]. At present, a variety of SERS arrays substrates have been fabricated by different approaches including nanosphere lithography (NSL), electron lithography technique and anodic aluminum oxide (AAO) template method [17–18]. In comparison, photo-lithography is a simple, low-cost and easy available route for fabricating a uniformly high-ordered and large scale microstructure arrays [19], by which the periods and morphologies of noble metal arrays can be tuned flexibly combining the electrodeposition self-assembly [20–21].

In this paper, we present a simple approach for fabricating the highly ordered Au-Ag alloy arrays in silicon pillar substrates by photolithography and coelectrodeposition self-assembly, and subsequently demonstrate the good control in the morphologies of the Au-Ag alloy structure by means of adjusting the nucleation and growth processes via changing the applied voltage and reaction time. In particular, the Au-Ag alloy prepared can grow tightly on the silicon pillar substrate, which can be recycled after being cleaned in the organic solvent. Moreover, large scale silicon pillar substrates can be obtained very quickly by photolithography and XeF_2 dry etching, where the highly selective isotropic Silicon etch rates are 1–2 μm per minute. Therefore, we think that our result provides a new approach towards ordered arrays of alloy plasmonic structures and makes a demonstration of the emergent application of photolithography and coelectrodeposition self-assembly in SERS substrates for single-molecule detection.

2. Experimental

The fabrication procedure for the Au-Ag alloy arrays can be seen in Fig. 1 (a) and the detail process is as follows: Firstly, a layer of photoresist (AZ MiR (TM) 701 Photoresist) is coated on silicon wafers by spin coating, and then baked at 90 °C for 15 min. After being exposed in a mask aligner (MJB 3, SUSS MicroTec), the silicon wafer coated by photoresist is immersed in developing solution (AZ 300 MIF developer, Made in South Korea) and rinsed by deionized water. Subsequently, a XeF_2 dry etcher systems is adopt to isotropically etch the silicon for less than one minute, and then the high ordered silicon pillar arrays are obtained after cleaning up the residual of photoresist by acetone. Finally, the Au-Ag alloy grows on these silicon arrays by coelectrodeposition and self-assembly with the $HAuCl_4$ and $AgNO_3$ mixed aqueous solution as electrolyte. The morphologies of Au-Ag alloy have been tailored by controlling the nucleation and growth processes through careful regulation of reaction rate via changing the applied voltage and reaction time.

The morphology of the Au-Ag alloy arrays are characterized by a scanning electron microscope (SEM: SU8010, Hitachi), and the effect of morphology on the SERS properties are demonstrated by measuring the Raman spectra of alloy arrays with different morphologies using a HORIBA Jobin Yvon LabRAM HR Evolution cofocal microprobe Raman spectrometer with the 532 nm He-Ne Laser line at room temperature and the diameter of the focused laser spot is about 2 μm. Samples for SERS are dipped into the Rhodamine 6G (R6G) aqueous solution with concentrations of 10^{-5} M for 10 h, followed by thorough rinsing in deionized water to remove the unbound R6G molecules and dry before SERS measurement.

3. Results and discussion

Fig. 1(b) shows the highly ordered silicon pillar arrays fabricated by photolithography and dry etching, with the smooth surface and extremely rough groove bottom. Owing to the superhydrophobic properties of the silicon pillar as the coelectrodeposition electrode (the contact angle (CA) is about 109.3°, as shown in the S1), air pockets are trapped inside structural gaps [22], which cause the restrictive contact between electrolyte and pillar tops. Thus the dendritic Au-Ag alloy can be reduced and assembled mostly upon the pillar top surfaces, while few fragmentary alloy nano dots can be obtained on the bottom of the arrays. The measured EDS mapping indicates that the distribution of the Ag and Au element is uniform as shown in the S2 in the Supplementary Material.

In this process, preferential growth of Au - Ag alloy arrays on silicon pillar structure has been investigated by changing the applied voltages, as shown in Fig. 2.The voltage of Fig. 2(a), (b), (c), (d), (e) and (f) is 4 V, 9 V, 14 V, 19 V, 24 V and 29 V, respectively. It is obvious that the applied voltage plays a powerful role in the growing process of Au-Ag alloy. According to the diffusion limited aggregation (DLA) model, during the reduction and growth process, aggregation number and size can determine anisotropic morphology of Au-Ag alloy [23–24]. As seen from the Fig. 2, when the voltage is low such as less than 4 V (Fig. 2(a)), due to the insufficient electrons provided and low nucleation speed, few Au-Ag alloy can be deposited on the silicon substrate. With the increasing of applied voltage, more and more electronics obtained obviously facilitates the nucleation and isotropic growth of the Au-Ag metal and uniform alloy arrays with flower-like hierarchy nanostructures form (as seen in Fig. 2(e)). However if the voltage is as high as 29 V, the nucleation is instantaneous, and massive metal ions are reduced to atoms, which can accelerate the isotropic growth steps, thereby isolated island Au-Ag alloy grain is formed as shown in Fig. 2(f).

The morphology evolution of Au-Ag alloy is a time-dependent process, as shown in the Fig. 3(a)-(d), the respective coelectrodeposition time is 5, 15, 25 and 30 min with the concentration of $HAuCl_4$ and $AgNO_3$ solution are 0.001 mM and the applied voltage is 24 V. Driven by the high enough voltage, The alloy ions near the cathode obtain the electrons and then to be reduced in the lowest energy part of the Si surface. With the increasing of the reaction time, these reduced alloy particles will grow and ripen, and the difference of alloy atoms on different crystal surfaces results in the increasingly visible anisotropic growth. Thereby flower-like alloy become bigger and denser (as shown in the Fig. 3(a)-(c)). At last, when the time is long enough (over 30 min), there are a few ripened tremendous dendrite, there is probably abnormal grain growth phenomenon of Au-Ag alloy and this tends to form a few ripened tremendous dendritic structures, which will restricts the growth of the surrounding Au-Ag alloy particles as seen in the Fig. 3(d). These extremely large dendritic structures cannot stick to the silicon substrate firmly. Therefore, in our experiment, the deposition time is controlled less than 30 min.

As SERS substrates, the flower-like Au-Ag alloy arrays prepared exhibit strong SERS effect by using 10^{-5}M R6G as probe molecules which can be observed from Fig. 4(a) and (b) corresponding to different applied voltages from 4v to 29 V. Firstly, the contrast curve of the alloy arrays prepared on the Si pillar substrates and the flat Si wafer in Fig. 4(a) shows that the arrays present much stronger Raman signal, which is because that the extremely rough surface of alloy arrays can

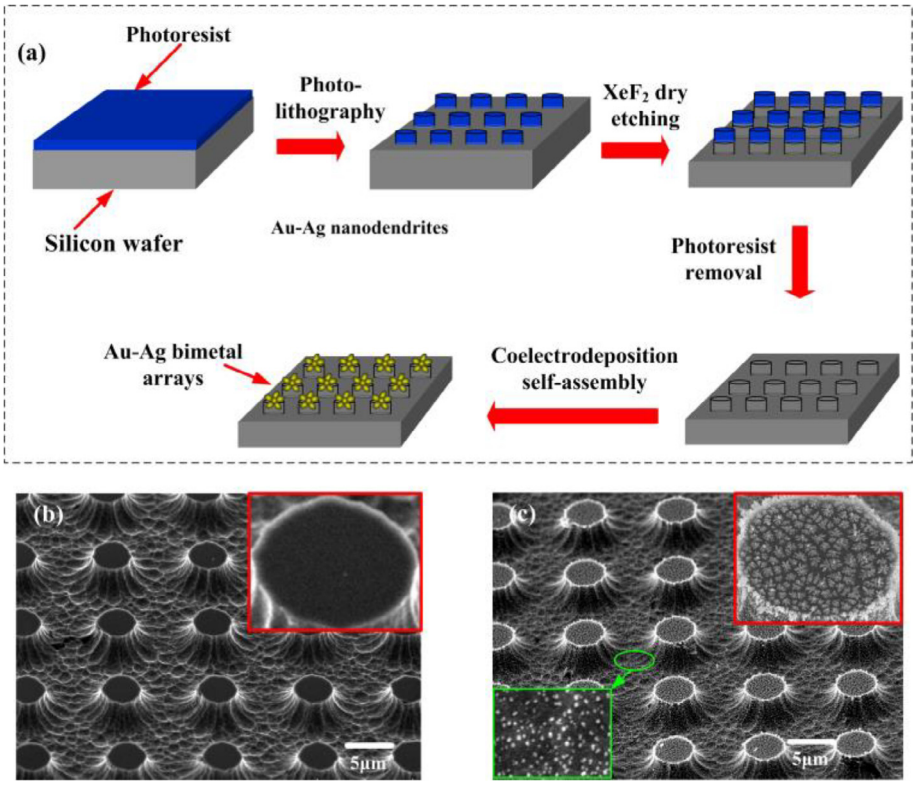

Fig. 1. The schematic for the fabrication of Au-Ag alloy arrays (a), and the SEM images of the silicon pillar arrays (b) and the Au-Ag alloy arrays (c).

absorb more R6G probe molecules and further enhance the intensity of Raman signal. The Au-Ag alloys on the Si pillar substrates and the flat Si wafer both are prepared in the same experimental condition, the SEM images of which can be seen in S3 of the Supplementary Material. Moreover, it is also perfectly reasonable to come to that the microscopic morphologies have a key influence on the intensity of Raman signals (see the insert curves in Fig. 4(b)). Arrays under lower deposition voltage with less flower-like Au-Ag alloy is of weaker SERS signal. With the increasing of the voltage, much-branched flower structure with more corners and edges are growing leading to numerous contacts and interaction, which can provide more Raman “hot spots” and make Raman light radiate more efficiently into free space, therefore enhance the SERS effects [25–26]. While when the applied voltage is 29 V, the Raman signal decreases, due to the isolated island morphologies of the arrays.

This enhancement can also be deduced from the theoretical simulation of electric field' spatial distribution. Fig. 4(c) and (d) show the spatial distribution of electric field for flower-like and spherical metal arrays, respectively, by three dimensional finite-difference time-domain (3D FDTD) simulations (Lumerical FDTD Solution, Inc., Canada). The total field/scattered-field plane wave source with the wavelength of 532 nm is selected and the polarization direction is parallel to the horizontal direction. As seen from the Fig. 4(c) and (d), it is obvious that the electromagnetic field (EM) enhancement in the gaps generated from the flower-like nanostructure is larger than the spherical-like nanostructure, which means that the enhancement factor consistent with

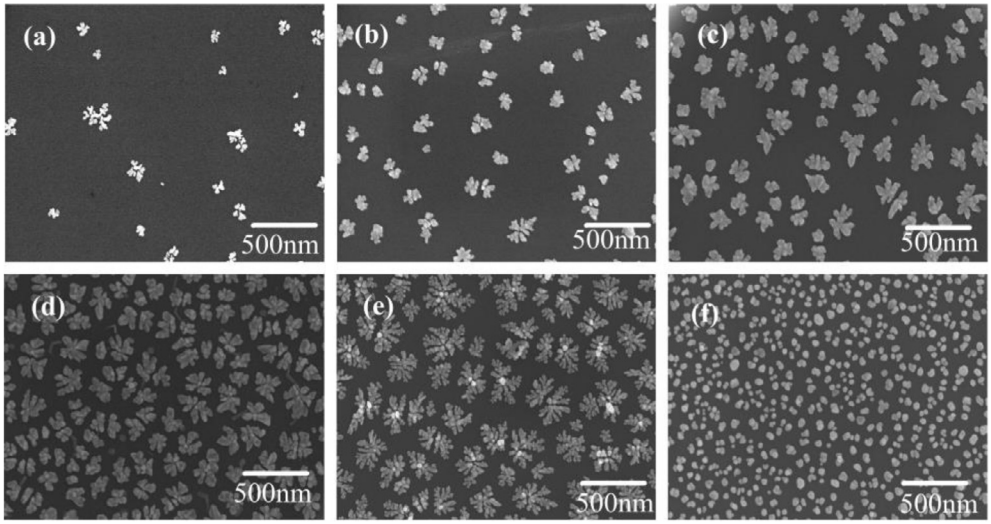

Fig. 2. SEM images of the Au-Ag alloy arrays on Si pillar strucuture prepared with different applied voltage. The voltage of (a), (b), (c), (d), (e) and (f) is 4 V, 9 V, 14 V, 19 V, 24 V, 29 V, respectively. The concentration of HAuCl4 and AgNO3 solution are 0.001 mM and the deposition time is 10 min.

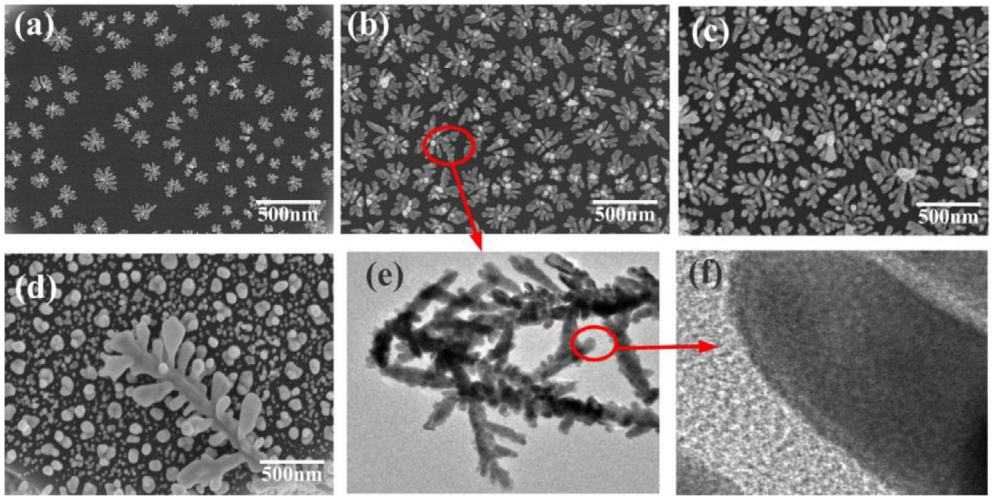

Fig. 3. SEM and TEM images of the Au-Ag alloy on silicon pillar substrate prepared with different deposition time. The time of (a), (b), (c) and (d) is 5 min, 15 min, 25 min and 30 min, respectively. (e) is the TEM images of the flower-like Au-Ag alloy and their HRTEM images (f). The concentration of HAuCl4 and AgNO3 solution are 0.001 mM and the applied voltage is 24 V.

the SERS spectra is stronger.

In order to validate the SERS enhancement of flower-like Au-Ag alloy on the top of the highly ordered arrays, the compared Raman spectra of the R6G absorbed on the top and bottom of the arrays are measured, as shown in the Fig. 5. Here, curve (a) and (b) in Fig. 5 are the spectra tested on the top and bottom of the arrays, respectively, from which it can be seen that the Raman intensity of the flower-like Au-Ag alloy on the top surface is much stronger than that on the bottom. Therefore, it can be deduced that the SERS enhancement is mainly derived from the tops of Au-Ag alloy arrays.

Fig. 6(a) shows the typical Raman spectra of the R6G absorbed on Au-Ag alloy arrays with different composition of Au^{3+}-Ag^{+} contained in the original electrolyte, excited by the 532 nm laser line, which present clearly the dependences of the SERS intensity on alloy composition. The SERS signals increase firstly with the increasing of Au^{3+} composition and then decrease, and the maximum count point appears in the 1:1 mol ratio of Au^{3+}: Ag^{+}, where the final atom ratio of Au and Ag is about 12: 88 according to the EDS result (see Fig. 6(c)). The SERS spectra for as-prepared Au-Ag alloy with the 1:1 mol ratio of Au^{3+}: Ag^{+}

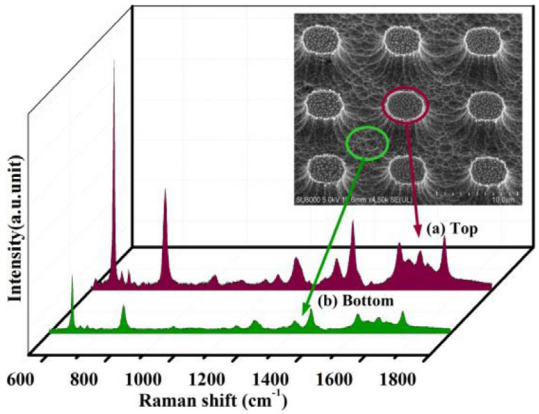

Fig. 5. SERS spectra for different areas of Au-Ag alloy arrays probed with 10^{-5} M R6G. Here, curve (a) is the SERS spectrum measured on the top of the Si pillar, and curve (b) is the SERS spectrum measured on the bottom of the Si pillar.

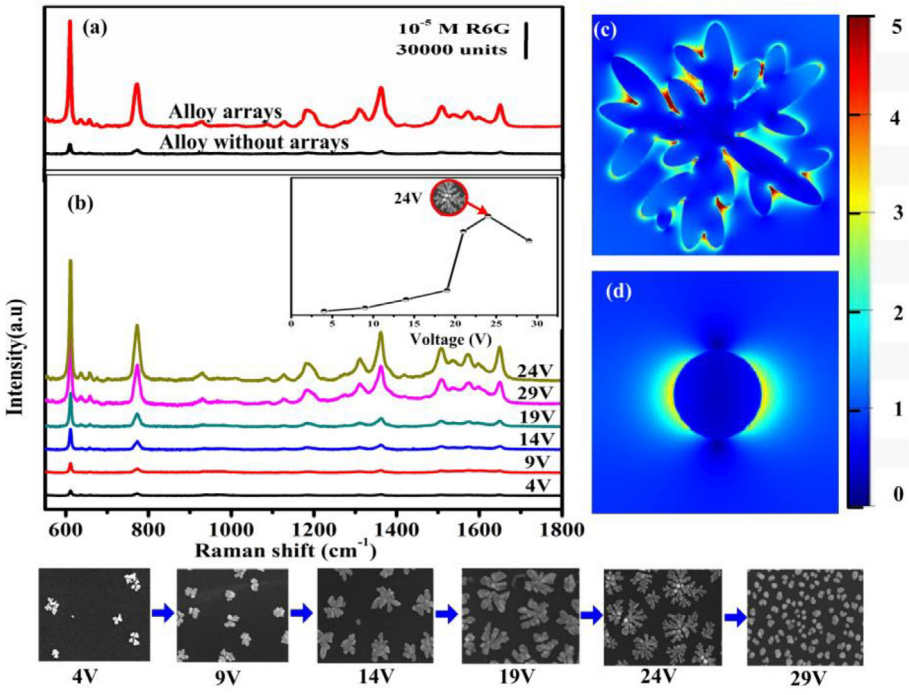

Fig. 4. SERS spectra for as-prepared Au-Ag alloy arrays probed with R6G. Here, Fig. 4(a) is the SERS contrast curve of the alloy prepared on Si pillar arrays and on the flat Si wafer and the Fig. 4(b) are SERS spectra probed with 10^{-5} M R6G corresponding to the Au-Ag arrays shown in Fig. 2 at different applied voltages (data integration time: 5 s). Fig. 4(c) and (d) is the spatial distribution of the electric field obtained by 3D FDTD simulation for flower-like and spherical metal arrays, respectively.

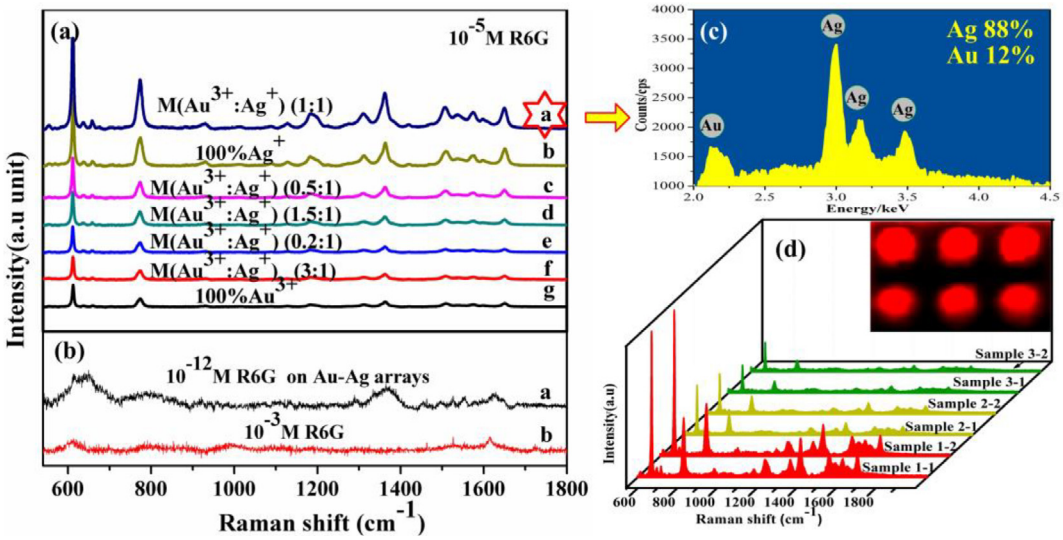

Fig. 6. SERS spectra of Au-Ag alloy arrays probed with R6G (data integration time: 3 s). Here, (a) is the contrast curve of Au-Ag arrays with the different mole ratio of Au^{3+} and Ag^{+} in the electrolyte. (b) is the SERS spectrum probed with 10^{-12} M R6G absorbing on the Au-Ag arrays (curve a) and the normal Raman peaks for 10^{-3} M R6G (curve b), respectively. (c) is the EDS result corresponding to the Au-Ag alloy with the 1:1.mole ratio of Au^{3+} and Ag^{+}. (d) is the reproducibility of the samples selected randomly for SERS test, where the inset image is the Raman mapping of the R6G at 613 cm^{-1}.

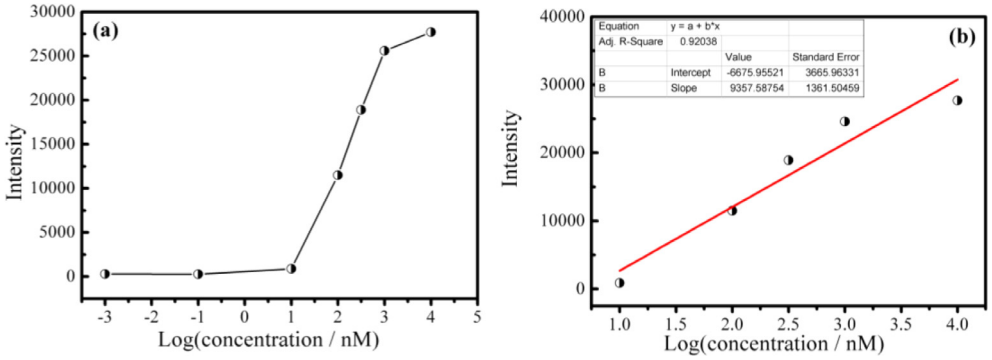

Fig. 7. SERS detection of R6G with the as-prepared Au-Ag alloy arrays. Here, (a) is the averaged peak intensities of the 612 cm^{-1} band as a function of the logarithmic concentration of R6G, and (b) is the calibration curve where the peak intensity measured at 612 cm^{-1} is plotted versus the logarithmic concentration of R6G.

and 100%Au probed with 10^{-5} M R6G are also tested with the 633 nm laser, as shown in the S4, from which it can be seen that the Au-Ag alloy also shows the better SERS enhancement. Therefore, the maximum SERS enhancement should be relate to the two metal -molecules interaction. A small amount of Au (12%) in the isomorphous - phase alloy leads to a charge separation that will favor its adsorption to the silver domains, which should increase the surface concentration of R6G molecules leading to an increase in SERS intensity [27]. Moreover, because the Au-Ag alloy prepared on the silicon pillar substrate can grow tightly, the Raman measures for these alloy array SERS substrates hold high repeatability and stability properties. As seen in Fig. 6(d), some samples identified as sample 1, sample 2 and sample 3 are picked up randomly for SERS detection under the same measure condition, and the second set of results is virtually the same as the first for each sample. Meanwhile, the inset Raman mapping in the Fig. 6(d) of the sample 1–1 can also indicate the good reproducibility of one sample.

In our paper, under the optimal SERS enhancement condition, the R6G with the concentration as low as 10^{-12} M can be detected (as shown in the Fig. 6(b)). The enhancement factor (EF) of Au-Ag alloy arrays is estimated through the following equation [28]:

$$EF = \frac{I_{SERS}}{I_{Normal}} \times \frac{C_{SERS}}{C_{Normal}}$$

Here, I_{SERS} and I_{Normal} is the intensity of SERS spectrum and normal spectrum of R6G and the C_{SERS} and C_{Normal} is the concentration of R6G, respectively. Both the SERS and Raman measurements are performed under the same conditions. We measure the SERS peak at 1615 cm^{-1} for 10^{-12} M R6G absorbing on the Au-Ag alloy arrays and the normal 10^{-3} M R6G, as shown in Fig. 6(b), The EF is estimated to be 1.2×10^{9}.

The limit of detection (LOD) for R6G is calculated for the further evaluation of the sensitivity of the Au-Ag alloy array, which is defined as the concentration at which the signal-to-noise ratio is equal to 3 [29]. The SERS peak at 612 cm^{-1} is measured for the R6G with several different concentrations (as seen in the Fig. 7), and The LOD of R6G is calculated to be 5.8×10^{-9} M for the Au-Ag alloy arrays.

4. Conclusions

In conclusion, assisted by the electrochemical reaction self-assembly and photolithography, a simple process has been demonstrated for the controlled and reproducible fabrication of a highly ordered Au-Ag alloy arrays for SERS. The SERS enhancement is related to the microscopic morphologies and well as the composition the of the Au-Ag alloy. Maximum SERS is observed for the alloy much-branched flower-like Au-Ag structure with the 12%Au and 88%Ag, due to its wealthy corners and edges that provide plentiful Raman “hot spots”. Meanwhile, the small amount of Au (12%) in the bimetal alloy will favor the adsorption of R6G probe molecules to the silver domains, which should also increase the SERS intensity. The FDTD simulations of the field distribution are also studied and the result is in good agreement with experiments. This fabrication method can be applied to fabricating other noble metal arrays structures towards the sensitive SERS substrates and

single-molecule detection.

Acknowledgements

The authors acknowledge the financial supports from the National Natural Science Foundation of China (Nos. 51202033, 11204039 and 51502037), the Natural Science Foundation of Fujian Province of China (Nos. 2016J01213, 2015J01243 and 2015J01399) and the Science Foundation of the Educational Department of Fujian Province of China (No. JA13084).

Appendix A. Supplementary data

Supplementary data associated with this article can be found, in the online version, at http://dx.doi.org/10.1016/j.cej.2018.03.192.

References

[1] M. Fleischmann, I.R. Hill, J. Robinson, Surface-enhnaced Raman scattering from silver electrodes Potencial and cation dependences of the very-low-frequency mode, Chem. Phys. Lett 97 (1983) 441–445.
[2] R.Z. Tan, A. Agarwal, N. Balasubramanian, D.L. Kwong, Y. Jiang, E. Widjaja, M. Garland, 3D arrays of SERS substrate for ultrasensitive molecular detection, Sensor. Actuat. A: Phys. 139 (2007) 36–41.
[3] T. Chen, H. Chen, H. Wang, G. Chen, Y. Wang, Y. Feng, W.S. Teo, T. Wu, and Hotspot-Induced Transformation of Surface-Enhanced Raman Scattering Fingerprints, Acs Nano 4 (2010) 3087–3094.
[4] H. Tang, G. Meng, Q. Huang, C. Zhu, Z. Huang, Z. Li, Z. Zhang, Y. Zhang, Urchin-like Au-nanoparticles@Ag-nanohemisphere arrays as active SERS-substrates for recognition of PCBs, RSC Adv. 4 (2014) 19654–19657.
[5] P. Huang, Z. Wang, L. Lin, Z. Feng, X. Wen, Z. Zheng, Self-assembled dendrite Ag arrays with tunable morphologies for surface-enhanced Raman scattering, Appl. Surf. Sci. 386 (2016) 345–351.
[6] S.B. Chaney, S. Shanmukh, R.A. Dluhy, Y.P. Zhao, Aligned silver nanorod arrays produce high sensitivity surface-enhanced Raman spectroscopy substrates, Appl. Phys. Lett. 87 (2005) 031908.
[7] B. Chen, G. Meng, F. Zhou, Q. Huang, C. Zhu, X. Hu, M. Kong, Ordered arrays of Au-nanobowls loaded with Ag-nanoparticles as effective SERS substrates for rapid detection of PCBs, Nanotechnology 25 (2014) 145605.
[8] Z. Wang, Z. Feng, L. Lin, P. Huang, Z. Zheng, Top-down patterning and self-assembly of flower-like gold arrays for surface enhanced Raman spectroscopy, Appl. Surf. Sci. 356 (2015) 1314–1319.
[9] D. Liu, C. Li, F. Zhou, T.Zhang, H. Zhang, X. Li, G. Duan,W. Cai, Y. Li, Rapid Synthesis of Monodisperse Au Nanospheres through a Laser Irradiation -Induced Shape Conversion, Self-Assembly and Their Electromagnetic Coupling SERS Enhancement, Sci. Rep. 5 (2015):7686.
[10] H.J. Yin, Z.Y. Chen, Y.M. Zhao, M.Y. Lv, C.A. Shi, Z.L. Wu, X. Zhang, L. Liu, M.L. Wang, H.J. Xu, Ag@Au core-shell dendrites: a stable, reusable and sensitive surface enhanced Raman scattering substrate, Sci. Rep. 5 (2015) 14502.
[11] H. Zhang, M. Liu, F. Zhou, D. Liu, G. Liu, G. Duan, W. Cai, Y. Li, Physical Deposition Improved SERS Stability of Morphology Controlled Periodic Micro/Nanostructured Arrays Based on Colloidal Templates, Small 11 (2015) 844–853.
[12] Y. Li, N. Koshizaki, H. Wang, Y. Shimizu, Untraditional Approach to Complex Hierarchical Periodic Arrays with Trinary StepwiseArchitectures of Micro-, Submicro-, nd Nanosized Structures Based on Binary Colloidal Crystals and Their Fine Structure Enhanced Properties, ACS Nano 5 (2011) 9403–9412.
[13] S.K. Cha, J.H. Mun, T. Chang, S.Y. Kim, J.Y. Kim, H.M. Jin, J.Y. Lee, J. Shin, K.H. Kim, a.S.O. Kim, Au-Ag core-shell nanoparticle array by block copolymer lithography for synergistic broadband plasmonic properties, Acs Nano 9 (2015) 5536–5543.
[14] R. Gillibert, M. Sarkar, J.F. Bryche, R. Yasukuni, J. Moreau, M. Besbes, G. Barbillon, B. Bartenlian, M. Canva, M.L. de la Chapelle, Directional surface enhanced Raman scattering on gold nano-gratings, Nanotechnology 27 (2016) 115202.
[15] C. Lee, C.S. Robertson, A.H. Nguyen, M. Kahraman, S. Wachsmann-Hogiu, Thickness of a metallic film, in addition to its roughness, plays a significant role in SERS activity, Sci Rep 5 (2015) 11644.
[16] H. Wei, H. Xu, Hot spots in different metal nanostructures for plasmon-enhanced Raman spectroscopy, Nanoscale 5 (2013) 10794–10805.
[17] Z. Huang, G. Meng, Q. Huang, Y. Yang, C. Zhu, C. Tang, Improved SERS performance from Au nanopillar arrays by abridging the pillar tip spacing by Ag sputtering, Adv. Mater. 22 (2010) 4136–4139.
[18] B. Chen, G. Meng, Q. Huang, Z. Huang, Q. Xu, C. Zhu, Y. Qian, Y. Ding, Green synthesis of large-scale highly ordered core@shell nanoporous Au@Ag nanorod arrays as sensitive and reproducible 3D SERS substrates, ACS Appl. Mater. Interfaces 6 (2014) 15667–15675.
[19] A. Shishido, I.B. Diviliansky, I.C. Khoo, T.S. Mayer, Direct fabrication of two-dimensional titania arrays using interference photolithography, Appl. Phys. Lett. 79 (2001) 3332–3334.
[20] J. Fang, B. Ding, X. Song, Self-assembly ability of building unitss in mesocrystal, structural, and morphological transitions in Ag nanostructures growth, Cryst. Growth & Des. 8 (2008) 3616–3622.
[21] X.-Y. Zhang, A. Hu, T. Zhang, W. Lei, X.-J. Xue, Y. Zhou, W. Duley, Self-Assembly of Large-Scale and Ultrathin Silver Nanoplate Films with Tunable Plasmon Resonance Properties, Acs Nano 5 (2011) 9082–9092.
[22] Y. Wu, K. Liu, B. Su, L. Jiang, Superhydrophobicity-mediated electrochemical reaction along the solid-liquid-gas triphase interface: edge-growth of gold architectures, Adv. Mater. 26 (2014) 1124–1128.
[23] T.A. Witten, L.M. Sander, Diffusion-limited aggregation, Phys. Rev. B 27 (1983) 5686–5697.
[24] F.L. Braga, O.A. Mattos, V.S. Amorin, A.B. Souza, Diffusion limited aggregation of particles with different sizes: Fractal dimension change by anisotropic growth, Physica A: Statistical Mechanics and its Applications 429 (2015) 28–34.
[25] Hye-Mi Bok, Kevin L. Shuford, Sungwan Kim, Seong Kyu Kim, a.S. Park, Multiple Surface Plasmon Modes for a Colloidal Solution of Nanoporous Gold Nanorods and Their Comparison to Smooth Gold Nanorod, Nano. Lett. 8 (2008) 2265-2270.
[26] H. Qian, M. Xu, X. Li, M. Ji, L. Cheng, A. Shoaib, J. Liu, L. Jiang, H. Zhu, J. Zhang, Surface micro/nanostructure evolution of Au–Ag alloy nanoplates: Synthesis, simulation, plasmonic photothermal and surface-enhanced Raman scattering applications, Nano Research 9 (2016) 876–885.
[27] M. Fan, F. Lai, H. Chou, W. Lu, B. Hwang, A.G. Brolo, Surface-enhanced Raman scattering (SERS) from Au: Ag bimetallic nanoparticles: the effect of the molecular probe, Chem. Sci. 4 (2013) 509–515.
[28] T. Zhang, F. Zhou, L. Hang, Y. Sun, D. Liu, H. Li, G. Liu, X. Lyu, C. Li, W. Cai, Y. Li, Controlled synthesis of sponge-like porous Au–Ag alloy nanocubes for surface-enhanced Raman scattering properties, J Mater. Chem. C 5 (2017) 11039–11045.
[29] C. Zhu, G. Meng, P. Zheng, Q. Huang, Z. Li, X. Hu, X. Wang, Z. Huang, F. Li, N. Wu, A Hierarchically Ordered Array of Silver-Nanorod Bundles for Surface-Enhanced Raman Scattering Detection of Phenolic Pollutants, Adv. Mater. 28 (2016) 4871–4876.